Published in IET Electric Power Applications
Received on 13th November 2013
Revised on 20th August 2014
Accepted on 22nd August 2014
doi: 10.1049/iet-epa.2014.0149

ISSN 1751-8660

Modelling and performance of a hybrid synchronous reluctance machine with adjustable X_d/X_q ratio

Linus U. Anih[1], Emeka S. Obe[1], Sylvester E. Abonyi[2]

[1]*Department of Electrical Engineering, University of Nigeria, Nsukka, Enugu State, Nigeria*
[2]*Department of Electrical and Electronic Engineering, Nnamdi Azikiwe University, Awka, Anambra State, Nigeria*
E-mail: simon.obe@unn.edu.ng

Abstract: Analytical and experimental studies of a hybridised synchronous reluctance machine with a variable X_d/X_q ratio characteristic is the subject of this study. The machine comprises a round rotor and a salient pole machine element that is mechanically coupled together and integrally wound. There are two sets of poly-phase windings in each stator. The windings of one of the sets are transposed between the two sections of the machine. Either set of the windings may be connected to the supply while the other feeds a balanced capacitance load. It is shown that by tuning of the capacitance load that the X_d/X_q ratio varies theoretically from zero to infinity at very good power factors. The machine characteristics were verified using the generalised two-axis theory and validated by experimentation. The experimental and analytical results obtained show good agreement. Saturation was investigated by using the variation of the d-axis inductance with machine loading. A set of rotor windings may be introduced for the purpose that the machine be self-starting and self-synchronising as a motor. The rotor field windings when fed with dc, will make the machine also capable of operation as a stand-alone salient-pole generator. For this purpose, it was shown that for a very high saliency ratio, reluctance power can be considerably higher than the excitation power.

1 Introduction

Reluctance machines comprise basically a stator, with current carrying windings which produce a rotating magnetic field as in induction motors, and a second member, the rotor, which is magnetically anisotropic; that is, the reluctance to the passage of flux along one axis is a minimum and along a second axis, at 90 electrical degrees to the first is a maximum. The operation of the machine depends on the tendency of the low-reluctance axis to align itself with the axis of the rotating magnetic field.

Reluctance machines occupy a very lowly position in the family of rotating electrical machinery because of its low output power and power factor in comparison with an induction machine of the same dimensions, the output being about one-third of the former. Despite these disadvantages, reluctance motors are almost the inevitable choice in electric clocks, textile drives, synchronous switches drives and so on. Among more sophisticated applications are their uses to position control rods precisely and reliably in nuclear reactors, and as slave motors in multi-machine systems requiring exact synchronisation of all elements at all times.

Various attempts have been made to improve the output power of the machine by ingenious design and re-design of the rotor structure [1]. The attempts were aimed at enhancing the X_d/X_q ratio on which the output power depends which essentially means reducing the q-axis reactance. The major difficulty of enhancing the X_d/X_q ratio by reduction of the q-axis reactance is that there is always an attendant decrease in X_d as well; resulting in a X_d/X_q ratio which is less than the bargained. Other consequences of this are an increase in the no-load current of the machine and synchronisation problems in line-start applications.

Capacitors have been known for ages as power factor improvement element in ac systems. To improve the power factor of an electrical machine by connecting a capacitor to it, another winding is required. This is because if a capacitor is connected in series with the machine winding, its inductive reactance which is responsible for energy conversion will be altered. A parallel connection will aid the power factor of the mains supply and have a very minimal effect on the machine. For this reason, a second winding is therefore needed. This second winding makes the machine look like its single-phase counterpart in which the main winding is connected to the supply and the auxiliary winding to the capacitor. A number of such studies have been performed by many researchers. The first report of such a scheme is the 'Wanlass motor' invented by Wanlass [2]. This scheme connects the two stator windings (of same pole number) of an induction motor directly to the source but with one of the windings displaced 60° (electrical) from the other and connected in series with a capacitor. This induction motor was later proven by Umans and Hess [3] to be inefficient. The second report is the 'unity-plus winding motor' invented by Roberts [4] with claims of better efficiency than the Wanlass motor. Its connection scheme is different as only one winding set is

connected to the supply and the other connected to capacitor only. The Robert's scheme was also subjected to a closer scrutiny by Medarametla *et al.* [5] who affirmed that it yields a power factor close to unity but not a better efficiency. One common feature of both the Wanlass and Roberts schemes is that both were applied to induction motors.

Sequel to this, the authors of this paper undertook the investigation of capacitor-assisted synchronous reluctance machines to ascertain the possibility of mitigating some of the key inherent deficiencies stated above. In [6–8], Obe and co-workers reported a replica of the Wanlass scheme as applied to line-start synchronous reluctance machines. This machine was seen to provide very good power factors especially at low load angles with reduced total losses at certain capacitance values. Anih and Agu [9] and Agu *et al.* [10] conceived and reported the exact scheme presented here but analysed the machine using semi-intuitive circuit theory approach based on machine impedances. Such approach did not provide sufficient information to allow a direct observation of quadrature and direct axes parameter variations with the load angle in the steady-state and run-up performance in the dynamic mode. Only a complete set of dynamic model equations derived through the theory of flux linkages and the well-known two-axis theory [11] will be capable of providing these needed details and which will make the machine more examinable and attractive. The authors are also aware of other two-winding synchronous machine schemes [12–14], although not assisted by capacitors but which report veritable findings similar to those presented here.

2 Machine description

An unconventional but simple machine configuration whereby the q-axis reactance can be varied without any deleterious effect on X_d is proposed in this paper. The machine consists essentially of a salient pole machine element coupled with a round rotor machine element; each machine has two sets of poly-phase stator windings. The windings of one set are transposed between the two sections of the machine. Either set of the windings may be connected to the supply while the other is connected to a variable balanced capacitor load bank. By simple tuning of the capacitance load, the X_d/X_q ratio can be theoretically varied from zero to infinity without manipulation of the rotor geometry at very good power factors including unity.

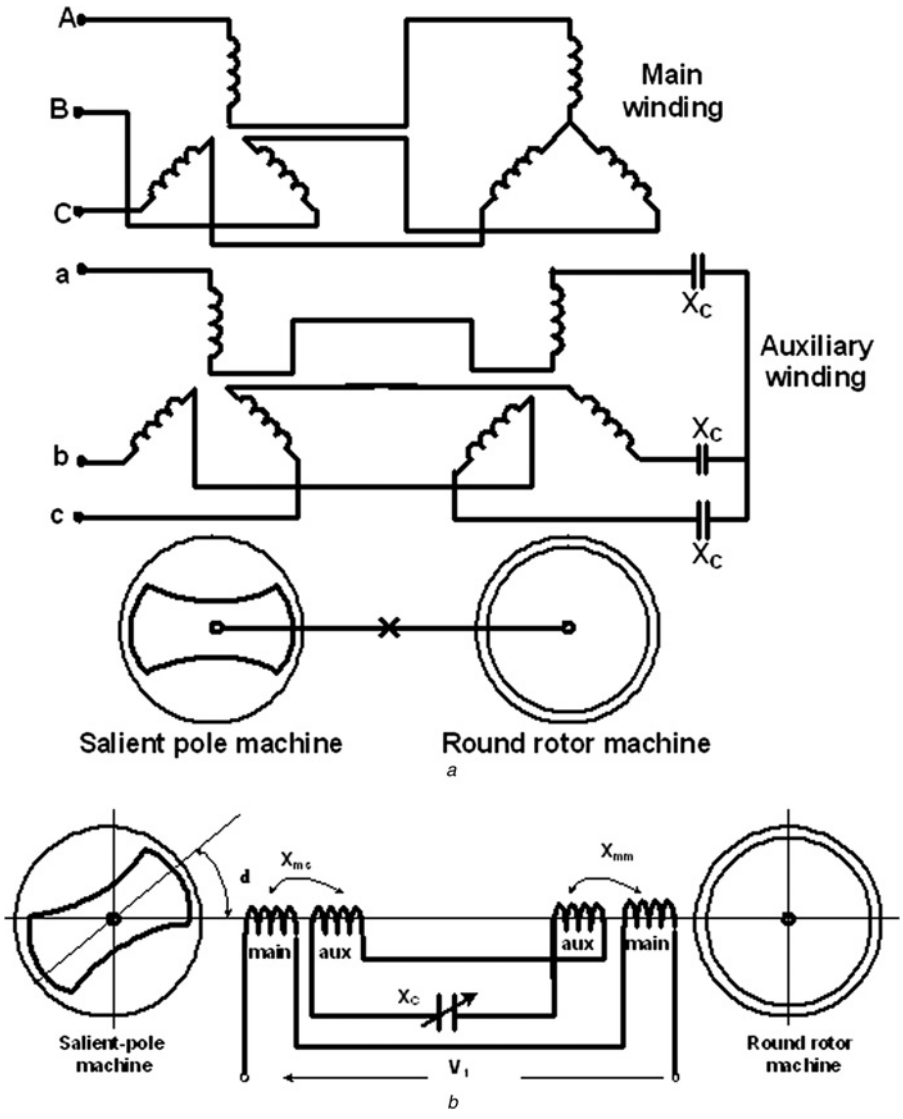

Fig. 1 *Connection diagram of the two machines*

a Connection diagram of the hybrid machine
b Per-phase connection circuit of the hybrid machine

IET Electr. Power Appl., 2015, Vol. 9, Iss. 2, pp. 171–182
doi: 10.1049/iet-epa.2014.0149

Fig. 1*a* shows the connection diagram of the two machines which will henceforth be called the 'hybrid machine'.

A simple three-phase transformer whose primary and secondary windings are identical with magnetising reactance X_m equal to the direct axis reactance X_d of the salient pole machine could conceptually replace the round rotor machine part for the purpose of reducing the entire rotor inertia and eliminating the need for coupling and all mechanical problems that may arise therefrom. This feature is only valid for the configuration discussed here (synchronous reluctance machine with no rotor conductors) as a round rotor machine with no rotor conductors will not be capable of contributing any torque and hence will not participate in the energy conversion process.

3 Machine model development

The model presented here is for a machine that has no rotor conductors as the primary interest here is the steady-state performance of the machine at differing capacitance values. The performance of the same is being closely studied in the dynamic regime for line-start applications and will form the subject of another paper. In the analysis that follows, upper case subscripts represent main winding terms while the lower case subscripts are for the auxiliary winding terms. The model developed relies on the usual assumptions of modelling synchronous machines as contained in classical texts [11, 15] and on the semi-intuitive per-phase circuit shown in Fig. 1*b*.

The dynamic model of this machine will be developed from Fig. 1*a*. The six voltage equations of the hybrid machine in stator reference frame can be written as

$$\boldsymbol{V}_{\mathrm{H}} = I_{\mathrm{H}}R_{\mathrm{H}} + \frac{\mathrm{d}\lambda_{\mathrm{H}}}{\mathrm{d}t} \tag{1}$$

where V_{H} represents the main and auxiliary winding voltages and is given in matrix form by

$$\boldsymbol{V}_{\mathrm{H}} = \begin{bmatrix} V_{ABC} V_{abc} \end{bmatrix} = \begin{bmatrix} V_A & V_B & V_C & V_a & V_b & V_c \end{bmatrix}^{\mathrm{T}} \tag{2}$$

The current matrix is given by

$$\boldsymbol{I}_{\mathrm{H}} = \begin{bmatrix} I_{ABC} & I_{abc} \end{bmatrix} = \begin{bmatrix} I_A & I_B & I_C & I_a & I_b & I_c \end{bmatrix}^{\mathrm{T}} \tag{3}$$

while the resistance matrix is

$$\boldsymbol{R}_{\mathrm{H}} = \mathrm{diag}\begin{bmatrix} R_A & R_B & R_C & R_a & R_b & R_c \end{bmatrix} \tag{4}$$

The flux linkage expression is

$$\begin{aligned} \lambda_{\mathrm{H}} &= \begin{bmatrix} L_{11} & L_{12} \\ L_{21} & L_{22} \end{bmatrix} \begin{bmatrix} I_{ABC} \\ I_{abc} \end{bmatrix} \\ &= \begin{bmatrix} L_{\mathrm{SS}} + L_{\mathrm{RR}} & L_{\mathrm{MS}} + L_{\mathrm{MR}} - 2L_L \\ L_{\mathrm{MS}} + L_{\mathrm{MR}} - 2L_L & L_{\mathrm{SS}} + L_{\mathrm{RR}} \end{bmatrix} \begin{bmatrix} I_{ABC} \\ I_{abc} \end{bmatrix} \end{aligned} \tag{5}$$

In (5), $\boldsymbol{L}_{\mathrm{SS}}$ is the 3×3 inductance matrix of the stator three-phase winding in the salient pole half of the machine, $\boldsymbol{L}_{\mathrm{RR}}$ is the 3×3 inductance matrix of the round rotor part of the machine. Each of $\boldsymbol{L}_{\mathrm{SS}}$ and $\boldsymbol{L}_{\mathrm{RR}}$ has their respective leakage parts in the appropriate places as in (6) and (8). On account of the assumption that the main and auxiliary windings are identical and both are mutually coupled and occupy the same slot positions, it follows that the mutual inductance between the two sets of windings are also equal. So in (5), $L_{\mathrm{MS}} = \boldsymbol{L}_{\mathrm{SS}}$ and $L_{\mathrm{MR}} = \boldsymbol{L}_{\mathrm{RR}}$. Finally, $\boldsymbol{L}_{\mathrm{L}}$ is the 3×3 leakage inductance matrices of any of the windings of either the round rotor or salient pole half of the hybrid machine which are also equal.

The inductance matrix for any of the two stator windings of the salient pole machine is well known from the literature [11] and is given as (see (6))

where

$$L_o = \frac{1}{3}\left(L_{md} + L_{mq}\right) \quad \text{and} \quad L_m = \frac{1}{3}(L_{md} - L_{mq}) \tag{7}$$

For the round rotor machine half of the machine, $L_{md} = L_{mq}$. This now implies that for this case, $L_o = (2/3)L_{md}$ and $L_m = 0$, so its stator winding inductance matrix can be shown from (6) to be

$$\boldsymbol{L}_{\mathrm{RR}} = \begin{bmatrix} L_{ls} + \frac{2}{3}L_{md} & -\frac{1}{3}L_{md} & -\frac{1}{3}L_{md} \\ -\frac{1}{3}L_{md} & L_{ls} + \frac{2}{3}L_{md} & -\frac{1}{3}L_{md} \\ -\frac{1}{3}L_{md} & -\frac{1}{3}L_{md} & L_{ls} + \frac{2}{3}L_{md} \end{bmatrix} \tag{8}$$

The leakage inductance matrix is

$$\boldsymbol{L}_L = \mathrm{diag}\begin{bmatrix} L_{ls} & L_{ls} & L_{ls} \end{bmatrix} \tag{9}$$

The sub-matrices of the inductance matrix of (5) can now be written out as (see equation (10) on the bottom of the next page)

and (see equation (11) on the bottom of the next page)

where

$$L_1 = L_{md} + \frac{1}{3}L_{mq} \quad \text{and} \quad L_2 = \frac{1}{2}L_{md} + \frac{1}{3}L_{mq} \tag{12}$$

$$L_{\mathrm{SS}} = \begin{bmatrix} L_{ls} + L_o - L_m \cos 2\theta_r & -\frac{1}{2}L_o - L_m \cos 2\left(\theta_r - \frac{\pi}{3}\right) & -\frac{1}{2}L_o - L_m \cos 2\left(\theta_r + \frac{\pi}{3}\right) \\ -\frac{1}{2}L_o - L_m \cos 2\left(\theta_r - \frac{\pi}{3}\right) & L_{ls} + L_o - L_m \cos 2\left(\theta_r - \frac{2\pi}{3}\right) & -\frac{1}{2}L_o - L_m \cos 2(\theta_r + \pi) \\ -\frac{1}{2}L_o - L_m \cos 2\left(\theta_r + \frac{\pi}{3}\right) & -\frac{1}{2}L_o - L_m \cos 2(\theta_r + \pi) & L_{ls} + L_o - L_m \cos 2\left(\theta_r + \frac{2\pi}{3}\right) \end{bmatrix} \tag{6}$$

A close observation of (10) and (11) in comparison with (6) shows that only the average value terms of the self and mutual inductances of the conventional synchronous machine were modified while the rotor position-dependent terms remain the same. Specifically, the average values of the self and mutual inductance terms improved by virtue of the connection of both stator windings by (2/3)L_{md} and (1/6)($L_{md}+4L_{mq}$), respectively.

From (10) and (11), it is evident that the inductance matrix of the hybrid machine is a function of rotor position and therefore, traditional transformation techniques using the matrix of (13) will be applied to relieve it of this dependence

$$T(\theta)=\frac{2}{3}\begin{bmatrix}\cos\theta & \cos\left(\theta-\frac{2\pi}{3}\right) & \cos\left(\theta+\frac{2\pi}{3}\right)\\ \sin\theta & \sin\left(\theta-\frac{2\pi}{3}\right) & \sin\left(\theta+\frac{2\pi}{3}\right)\\ 1/2 & 1/2 & 1/2\end{bmatrix} \tag{13}$$

This transformation at $\theta=\theta_r$ will be applied to (5) with (10) and (11) substituted as follows

$$\begin{aligned}\lambda_{\mathrm{QD}} &= \begin{bmatrix}T(\theta)L_{11}T(\theta)^{-1} & T(\theta)L_{12}T(\theta)^{-1}\\ T(\theta)L_{21}T(\theta)^{-1} & T(\theta)L_{22}T(\theta)^{-1}\end{bmatrix}\begin{bmatrix}I_{\mathrm{QD0}}\\ I_{qd0}\end{bmatrix}\\ &\equiv \begin{bmatrix}L_{\mathrm{QDS}} & L_{\mathrm{QDM}}\\ L_{\mathrm{QDM}} & L_{\mathrm{QDS}}\end{bmatrix}\begin{bmatrix}I_{\mathrm{QD0}}\\ I_{qd0}\end{bmatrix}\end{aligned} \tag{14}$$

where

$$L_{\mathrm{QDS}}=\begin{bmatrix}2L_{ls}+L_{md}+L_{mq} & 0 & 0\\ 0 & 2(L_{ls}+L_{md}) & 0\\ 0 & 0 & 2L_{ls}\end{bmatrix}\quad\text{and}$$

$$L_{\mathrm{QDM}}=\begin{bmatrix}L_{mq}-L_{md} & 0 & 0\\ 0 & 0 & 0\\ 0 & 0 & 0\end{bmatrix} \tag{15}$$

It is easy to observe that the d-axis and q-axis flux linkages for the two winding sets are

$$\lambda_{\mathrm{D}d}=\begin{bmatrix}\lambda_{\mathrm{D}}\\ \lambda_d\end{bmatrix}=\begin{bmatrix}2(L_{ls}+L_{md}) & 0\\ 0 & 2(L_{ls}+L_{md})\end{bmatrix}\begin{bmatrix}I_{\mathrm{D}}\\ I_d\end{bmatrix} \tag{16}$$

and (see (17))

From (16), it is clear that the overall d-axis inductances of the two windings sets are same and completely decoupled whereas the overall q-axis inductance matrix of (17) shows the existence of a coupling term. As will be seen later, this partly explains why the d-axis reactance of the machine remains constant when the capacitive loading of the auxiliary winding is changed while the q-axis reactance varies.

The voltage equation of the machine given in (1) above is same as that for any synchronous machine and it can be shown that the transformed voltage equations in the q–d rotor reference frame will still retain the traditional form

$$\begin{aligned}V_{\mathrm{Q}} &= 2r_s i_{\mathrm{Q}}+\omega_r\lambda_{\mathrm{D}}+\frac{\mathrm{d}\lambda_{\mathrm{Q}}}{\mathrm{d}t}\quad\text{and}\\ V_{\mathrm{D}} &= 2r_s i_{\mathrm{D}}-\omega_r\lambda_{\mathrm{Q}}+\frac{\mathrm{d}\lambda_{\mathrm{D}}}{\mathrm{d}t}\end{aligned} \tag{18}$$

$$\begin{aligned}V_q &= 2r_s i_q+\omega_r\lambda_d+\frac{\mathrm{d}\lambda_q}{\mathrm{d}t}+V_{cq}\quad\text{and}\\ V_d &= 2r_s i_d-\omega_r\lambda_q+\frac{\mathrm{d}\lambda_d}{\mathrm{d}t}+V_{cd}\end{aligned} \tag{19}$$

Equations (18) and (19) represent the voltages of the main winding and the auxiliary windings, respectively. Note that the auxiliary winding voltage equations have additional terms V_{cd} and V_{cq} added to them to account for the capacitor connected across it. In the d–q rotor reference frame, they are given by Obe [8] as

$$\frac{\mathrm{d}V_{cd}}{\mathrm{d}t}=\frac{i_d}{C}+\omega_r V_{cq}\quad\text{and}\quad\frac{\mathrm{d}V_{cq}}{\mathrm{d}t}=\frac{i_q}{C}-\omega_r V_{cd} \tag{20}$$

The dynamic equivalent circuit of the machine can now be drawn based on the above equations and is shown in Fig. 2.

$$L_{11}=L_{22}=\begin{bmatrix}2L_{ls}+L_1-L_m\cos 2\theta_r & -L_2-L_m\cos 2\left(\theta_r-\frac{\pi}{3}\right) & -L_2-L_m\cos 2\left(\theta_r+\frac{\pi}{3}\right)\\ -L_2-L_m\cos 2\left(\theta_r-\frac{\pi}{3}\right) & 2L_{ls}+L_1-L_m\cos 2\left(\theta_r-\frac{2\pi}{3}\right) & -L_2-L_m\cos 2(\theta_r+\pi)\\ -L_2-L_m\cos 2\left(\theta_r+\frac{\pi}{3}\right) & -L_2-L_m\cos 2(\theta_r+\pi) & 2L_{ls}+L_1-L_m\cos 2\left(\theta_r+\frac{2\pi}{3}\right)\end{bmatrix} \tag{10}$$

$$L_{12}=L_{21}=\begin{bmatrix}L_1-L_m\cos 2\theta_r & -L_2-L_m\cos 2\left(\theta_r-\frac{\pi}{3}\right) & -L_2-L_m\cos 2\left(\theta_r+\frac{\pi}{3}\right)\\ -L_2-L_m\cos 2\left(\theta_r-\frac{\pi}{3}\right) & L_1-L_m\cos 2\left(\theta_r-\frac{2\pi}{3}\right) & -L_2-L_m\cos 2(\theta_r+\pi)\\ -L_2-L_m\cos 2\left(\theta_r+\frac{\pi}{3}\right) & -L_2-L_m\cos 2(\theta_r+\pi) & L_1-L_m\cos 2\left(\theta_r+\frac{2\pi}{3}\right)\end{bmatrix} \tag{11}$$

$$\lambda_{\mathrm{Q}q}=\begin{bmatrix}\lambda_{\mathrm{Q}}\\ \lambda_q\end{bmatrix}=\begin{bmatrix}\left(2L_{ls}+L_{md}+L_{mq}\right) & -(L_{md}-L_{mq})\\ -(L_{md}-L_{mq}) & \left(2L_{ls}+L_{md}+L_{mq}\right)\end{bmatrix}\begin{bmatrix}I_{\mathrm{Q}}\\ I_q\end{bmatrix} \tag{17}$$

doi: 10.1049/iet-epa.2014.0149

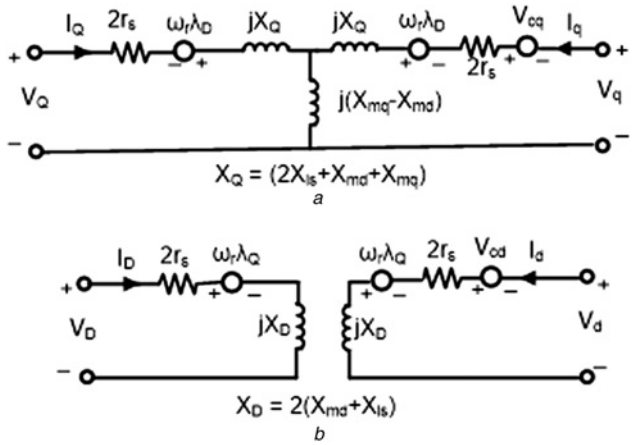

Fig. 2 *Dynamic equivalent circuit of the hybrid machine*

a *q*-axis
b *d*-axis

4 Steady-state model and equivalent circuit

For the purpose of examining the steady-state performance of this machine, the parameters of a 4-pole 2hp 220 V, 50 Hz, synchronous reluctance machine was used. It was not thought worthwhile to investigate this machine with variable frequency supplies as in [16] at this stage since the variation of supply frequency will eventually vary the values of axes reactances and capacitive reactances which govern the operation of the machine. To this end, only constant speed line-start operation is considered here. The unsaturated reactances are $X_{md} = 124.21\ \Omega$, $X_{mq} = 78.72\ \Omega$ and $X_{ls} = 12.0\ \Omega$. Since the stator windings of the machine are halved, the reactances were divided by a factor of 4 which now gave: $X_{md} = 31.05\ \Omega$; $X_{mq} = 19.67\ \Omega$ and $X_{ls} = 3.0\ \Omega$. The machine reactances (X_d and X_q) of the conventional reluctance machine were measured [17, 18] in terms of current. The dependence of X_d on load angle is needed in the next sections as load angle will be the operating parameter. This was realised as shown in Fig. 4*a* after both the reactance measurements and the load tests discussed in Section 5 from which a curvefit of the *d*-axis magnetising reactance, X_d was obtained as shown in (21). In the calculations that follow after the steady-state model development, the *d*-axis reactances were varied according to the saturation curve

$$X_d = \frac{1}{4}\left(10\delta^3 - 25\delta^2 + 5.9\delta + 29\right) \tag{21}$$

Under the steady-state operation in the rotor reference frame, all the time varying terms of (18)–(20) are set to zero and with (16) and (17) substituted, we have

$$V_{\mathrm{Q}} = 2r_s i_{\mathrm{Q}} + 2(X_{ls} + X_{md})I_{\mathrm{D}} \tag{22}$$

$$V_{\mathrm{D}} = 2r_s i_{\mathrm{D}} - \left(2X_{ls} + X_{md} + X_{mq}\right)I_{\mathrm{Q}} + \left(X_{md} - X_{mq}\right)I_q \tag{23}$$

$$V_q = 2r_s i_q + (2(X_{ls} + X_{md}) - X_c)I_d \tag{24}$$

$$V_d = 2r_s i_d - \left(2X_{ls} + X_{md} + X_{mq} + X_c\right)I_q + (X_{md} - X_{mq})I_{\mathrm{Q}} \tag{25}$$

There is no voltage supply to the second winding, therefore $V_d = V_q = 0$. Also, since the main winding is being supplied from balanced sinusoidal set of voltages [19]

$$V_{\mathrm{Q}} = V\cos\delta \quad \text{and} \quad V_{\mathrm{D}} = -V\sin\delta \tag{26}$$

where V is the rms value of the supply voltage and δ is the load angle.

When (26) is substituted into (21) and (22), they can be solved explicitly for I_{Q}, I_{D}, I_q and I_d in terms of V, r_s, X_{mq}, X_{md}, X_{ls}, X_c and δ. The resulting expressions for these axes currents are too long to be presented here.

At synchronous speed the steady-state mode, the following relations exist between the main and auxiliary windings rotor reference frame state variables and synchronously rotating phasors [11]

$$F_A = \left(F_{\mathrm{Q}} - jF_{\mathrm{D}}\right)e^{j\delta} \quad \text{and} \quad F_a = \left(F_q - jF_d\right)e^{j\delta} \tag{27}$$

where F can be current, voltage or flux linkage phasors. From the foregoing, the resulting steady-state per-phase equivalent circuit can be readily deduced and is shown in Fig. 3. In Fig. 3, it should be noted that $X_d = X_{md} + X_{ls}$.

It is now possible to assess the machine parameter variation in the steady-state using either (27) or Fig. 3.

4.1 Input impedance

The machine input impedance can be obtained by finding the ratio of the input voltage V_{AS} to the main winding current, I_{AS} employing (27) or by using simple circuit theory approach of looking into the input terminals of Fig. 3. Both approaches will naturally give the same results, however, for brevity we used the latter and the input impedance is given as

$$Z = 2\left(r_s + jX_d\right) + \frac{(2r_s + j(2X_d - X_c)) \times (X_{mq} - X_{md})\sin\delta e^{j\delta}}{(2r_s + \left(X_{mq} - X_{md}\right)\sin\delta e^{j\delta}) + j(2X_d - X_c)} \tag{28}$$

4.2 Theoretical axis reactances of the machine

In general, the impedance expression can be resolved to real (Re) and imaginary (Xe) terms. A plot of the real against the imaginary part of (28) for various values of X_c with δ ranging from 0 to π generates a family of circles as shown in Fig. 5. Each of these circles (impedance loci) has a constant *d*-axis reactance equal to $X_{\mathrm{D}} = 2(X_{\mathrm{ls}} + X_{\mathrm{md}})$ but the quadrature axis reactance X_{Q} varies being a function of a variable X_{C}.

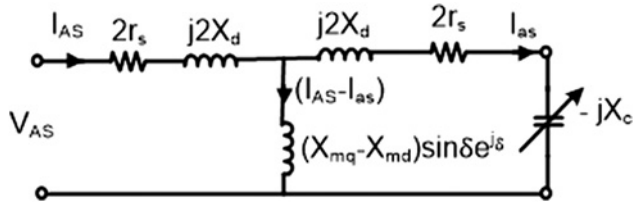

Fig. 3 *Per-phase steady-state equivalent circuit of the hybrid machine*

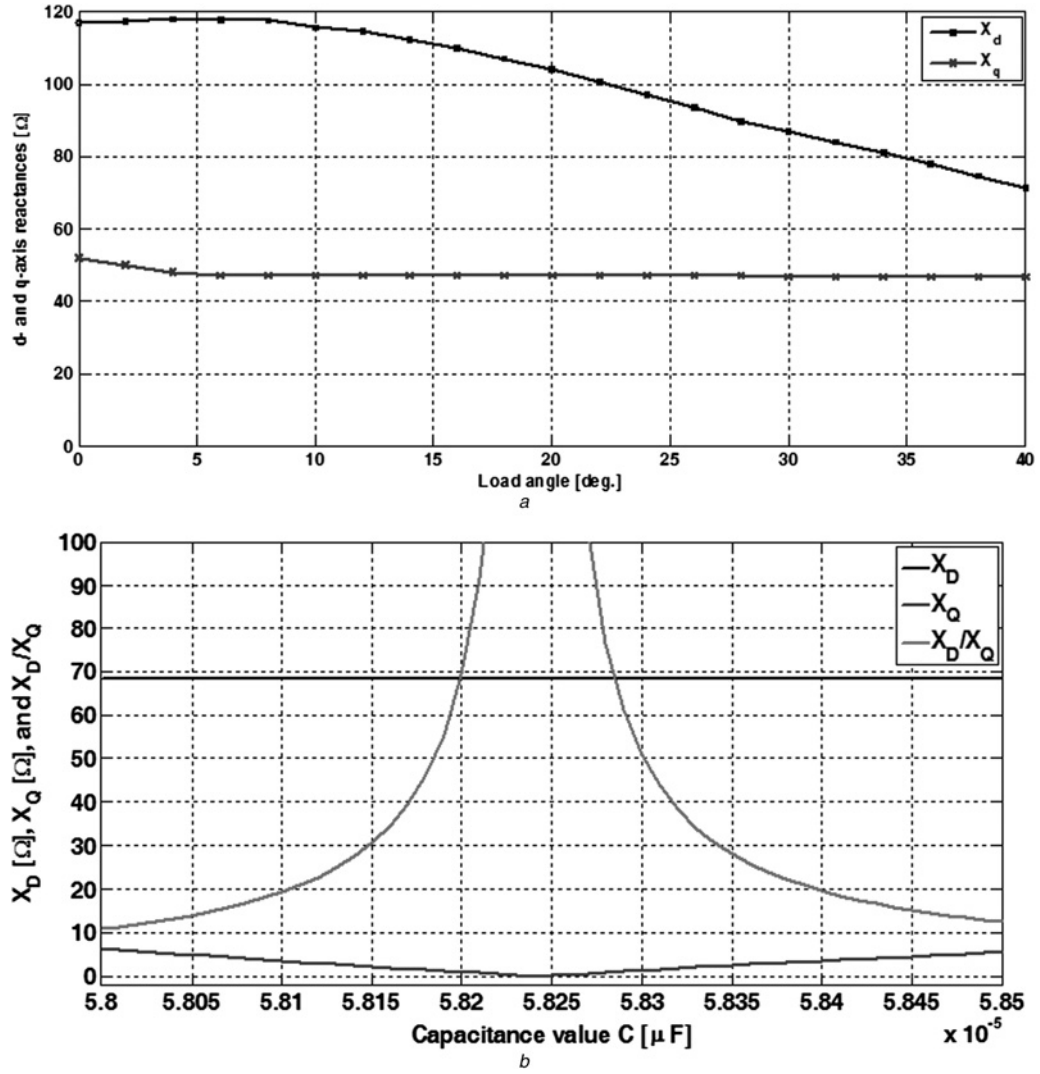

Fig. 4 *Reactance measurements, variation of axes reactances and X_d/X_q ratio with X_c*

a Measured variation of the *d*-axis and *q*-axis reactances for the conventional machine
b Variation of axis reactances and the reactance ratio with capacitance

4.2.1 Direct axis reactance: Using (28) in the limit that $\delta \to 0$ and for negligible stator winding resistance, the overall *d*-axis reactance is X_D and given by (29), which is clearly independent of the capacitive reactance

$$X_D = j2(X_{ls} + X_{md}) \tag{29}$$

4.2.2 Quadrature axis reactance: In the limit that $\delta \to \pi/2$ and for negligible stator winding resistance, the overall *q*-axis reactance is X_Q and given by

$$X_Q = j\frac{4X_{md}\left(X_{ls}+X_{md}+X_{mq}\right)+4X_{ls}-(2X_{ls}+X_{md}+X_{mq})X_c}{2X_{ls}+X_{md}+X_{mq}-X_c} \tag{30}$$

Evidently, it can be readily seen that only the effective quadrature axis reactance is influenced by the capacitance connected to the auxiliary winding. Consequently, variation of capacitive reactance varies the quadrature axis reactance X_Q only, while the direct axis reactance remains unaffected.

4.3 X_d/X_q ratio

The effective reactance ratio, X_D/X_Q of the hybrid machine can be closely examined by taking the ratio of (29) to (30). It is easier to visualise this reactance ratio graphically as shown in Fig. 4*b*, where for varying X_C, plots of X_D, X_Q and then X_D/X_Q are shown. In the plot, the values of capacitor (in μF) are given instead of X_C in order to justify that realistic values exist for even a value of the zero quadrature axis reactance. From (30), it can be shown that analytically, the zero quadrature axis reactance can be obtained when

$$X_c = \frac{4X_{md}(X_{ls}+X_{md}+X_{mq})+4X_{ls}}{2X_{ls}+X_{md}+X_{mq}} \tag{31}$$

For the machine under study this translates to a capacitance of about 58.23 μF.

4.4 Circle diagrams

Examination of (28) shows that the loci of Z for different values of capacitance loading of the auxiliary winding X_C

doi: 10.1049/iet-epa.2014.0149

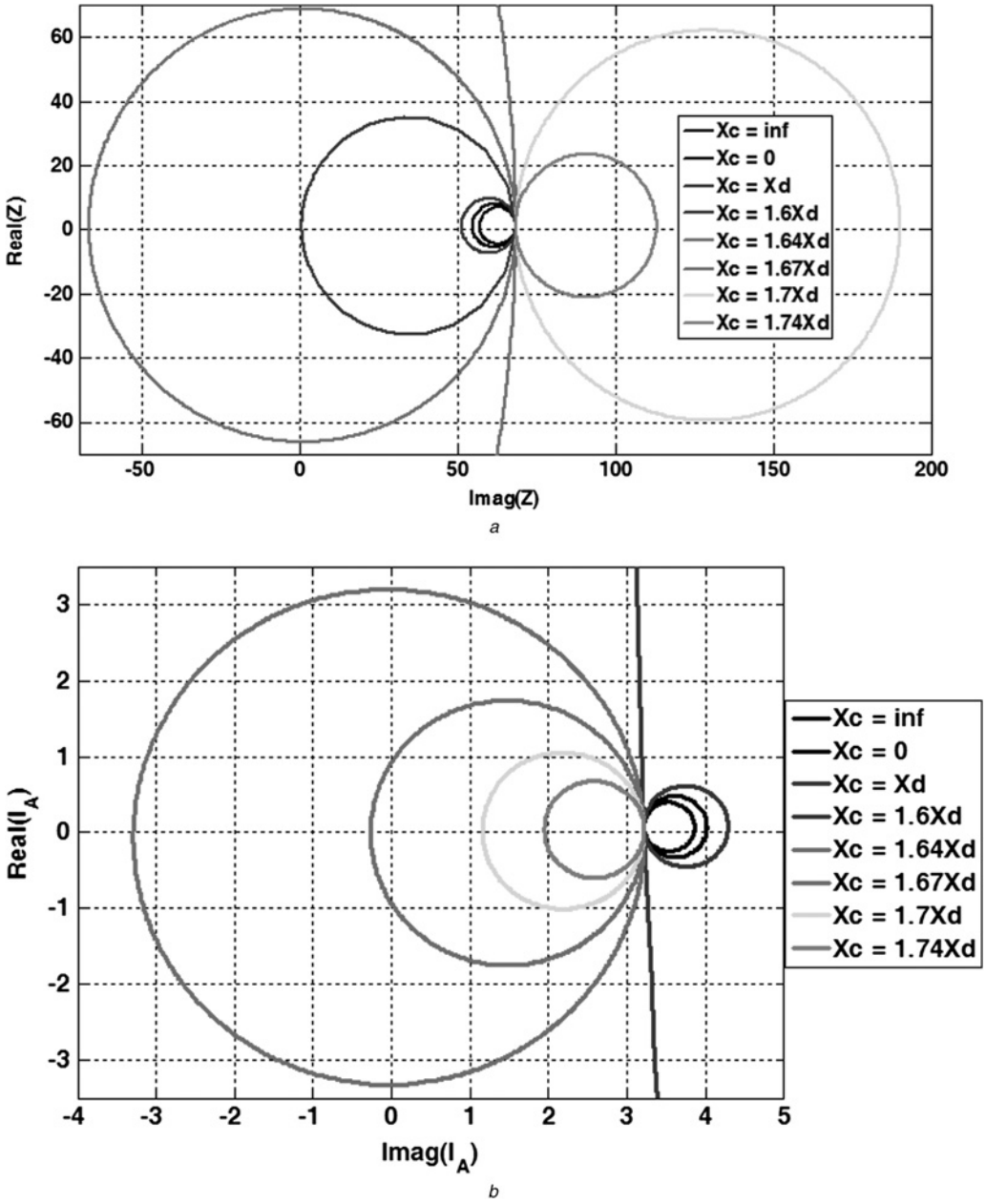

Fig. 5 *Variation of axis reactances and current as X_c changes*

a Impedance loci
b Current loci

as δ varies from 0 to π are family of circles with centre: [0, ½($X_D + X_Q$)] and radius ½($X_D - X_Q$) where X_Q is a variable parameter, which depends on X_C. All the circles are tangential to the line $X_D = 2X_d$. The quadrature axis reactance X_Q thus changes as X_C changes as shown in Fig. 5*a* while the *d*-axis reactance remains constant. For each impedance locus, there is a corresponding current locus. Each of the current loci is tangential to $I_{AS} = V_{AS}/(2X_d)$ point as shown in Fig. 5*b*. The centres of such circles will lie on the horizontal axis from $+\infty$ to $-\infty$. The *q*-axis reactance can even be negative and may be greater than X_D in magnitude.

The horizontal line Real(Z) = 0 which corresponds to Real(I_{AS}) = 0 as shown in Fig. 5 marks the transition of the machine from generating to motoring operations. At these points, the machine is neither motoring nor generating and the input power $VI\cos\varphi$ supplies the winding losses only.

It is observed from Fig. 5*a* that without the auxiliary winding ($X_C = \infty$), the value of $X_D = 68.3\ \Omega$ while the quadrature axis $X_Q = 56.9\ \Omega$, giving a very low X_D/X_Q ratio. The power factor and torque corresponding to these are also shown in Figs. 7*a* and *b*, respectively, and are also low.

When the auxiliary winding is introduced and short-circuited ($X_C = 0$), the diameter of the impedance locus increases, without changing the *d*-axis reactance X_D which remains constant at $X_D = 68.3\ \Omega$ while the quadrature axis reactance decreases to $54.7\ \Omega$; therefore giving a higher X_D/X_Q ratio over the open circuit case. There are torque and power factor enhancements as seen in the corresponding plots. The introduction of a variable capacitance load into the auxiliary winding makes the quadrature axis reactance X_Q variable and can be made to vary from zero to infinity. Some of the loci of the hybrid machine are of special interest.

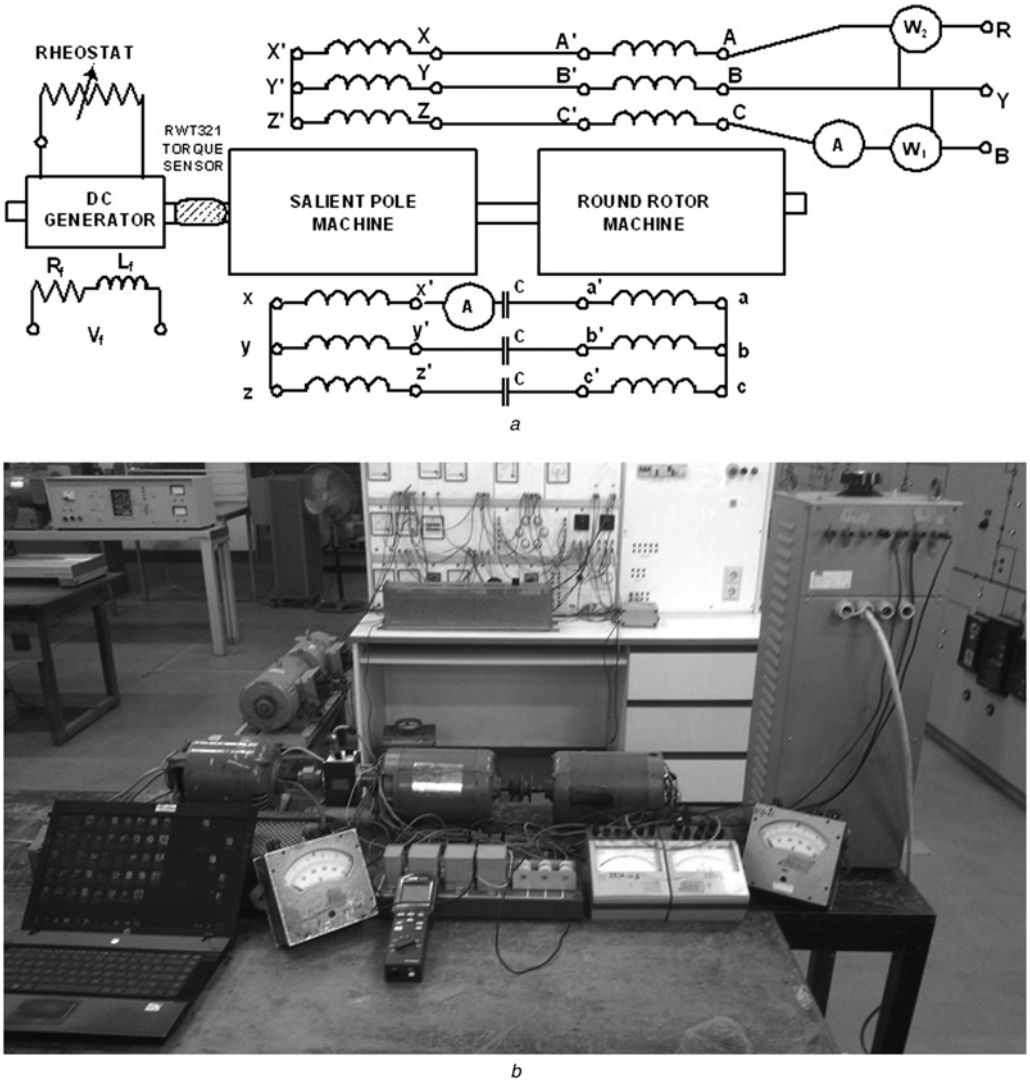

Fig. 6 *Layout of the experimental set-up used for measurements*
a Connection diagram
b Picture

For $X_C = 1.6X_d$, the quadrature axis reactance X_Q is completely neutralised, (i.e. $X_Q = 0$) by the capacitive reactance leading to infinitely high output power and unity power factor. Further increase in X_C between $1.6X_d$ and $1.67X_d$, X_Q becomes negative and the power factor becomes leading. For the capacitive reactance $X_C = 1.64X_d$, the centre of the impedance locus coincides with the origin, that is, $|-X_Q| = |X_D|$, the machine draws or supplies the same current irrespective of load. When the current loci embraces the third quadrant, the machine is able as a generator to supply lagging power factor loads and as a motor to supply leading power factor loads.

For $X_C = 1.67X_d$, X_Q is infinite and the corresponding current locus is $I_Q = 0$. The significance of this is that X_Q is now greater than X_D and the operating axis of the machine has shifted by $\frac{1}{2}\pi$ radians and the Q-axis have now become the no-load axis.

Between $X_C = 1.67X_d$ and $2X_d$, the impedance loci flip over to the right-hand side of the $X_Q = \infty$ axis, inductive in nature and shrinking. The shrinking of the flipped loci is because the capacitive reactance is becoming larger and thus increasing the impedance of the auxiliary winding towards the open-circuit case, which is inductive in nature and in consequence, the current in the auxiliary winding decreases. Although resistance was neglected in the plots, its inclusion would have shifted the impedance and current loci vertically upwards above the horizontal axis by an amount equal to the value of the resistance.

5 Experimental hybrid machine

Two identical units of 4-pole, 2hp, 220 V, 50 Hz, three-phase induction motors were acquired off the shelf. The effective axial length and rotor bore diameter are 85 and 92.5 mm, respectively. The stator windings of both machines were split into two equal parts identifiably as the main and auxiliary windings. The main windings were connected in series and the auxiliary windings connected in anti-series and either feeds a balanced capacitance load, is open circuited or short-circuited. Parts of the rotor of one of the machines were milled off to create a symmetrical 4-pole saliency with pole arc to pole pitch ratio of 0.6 while retaining the rotor cage with inter-polar end-ring connections. The main airgap, g_1 of 0.31 mm is retained as in the original induction motor and inter-polar slot space g_2, is cut down to 3.2 mm. A new round rotor without a cage was constructed for the second machine. To balance the

doi: 10.1049/iet-epa.2014.0149

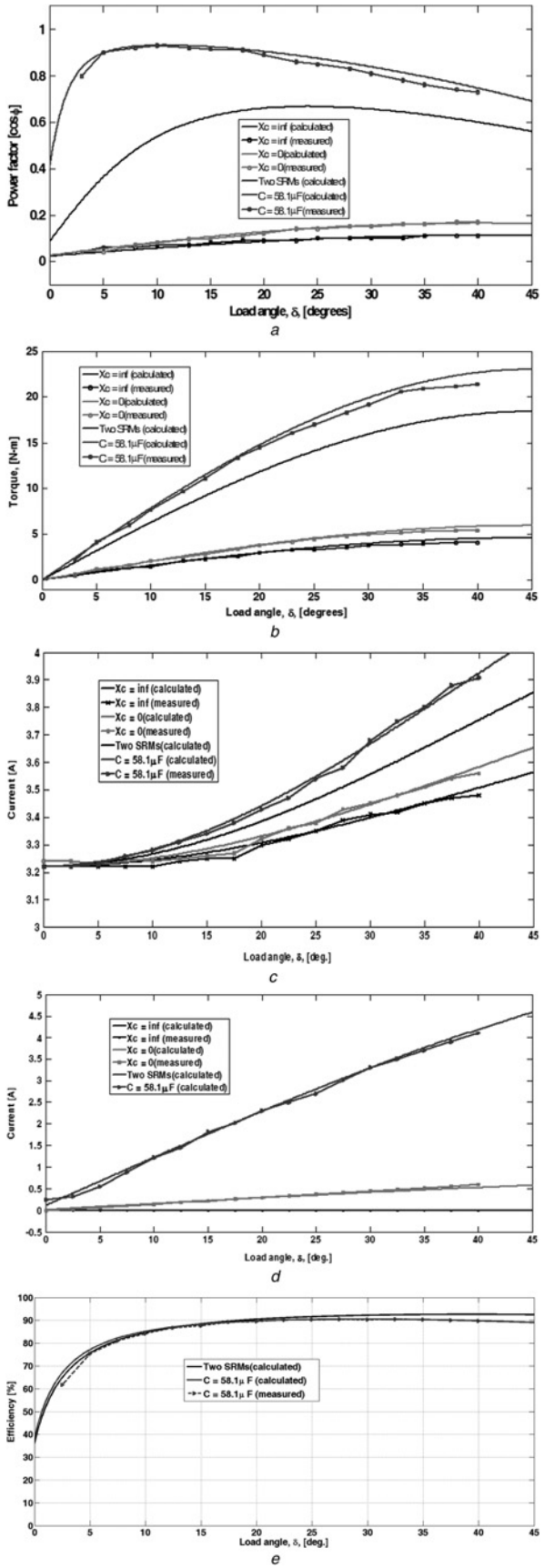

Fig. 7 *Presence of marginally higher power factors and torques rendered by the hybrid machine*

a Power factor plots
b Torque–angle plot of the hybrid machine
c Main winding current
d Auxiliary winding current
e Efficiency

reactances of the two machines, that is, to make the synchronous reactance of the round rotor machine equal the *d*-axis reactance of the second machine, two options are possible, (i) using different number of turns for the windings of the two machines (obviously, the salient pole machine will have a higher number) or (ii) using different values of airgaps. The second approach was used since a new rotor was made for the round rotor machine. This balance is achieved considering the reactances of the two machine halves. The *d*-axis reactance of the salient pole machine, X_d with T_{ph} turns per pole per phase and fundamental winding factor k_{w1} is given by [18, 20]

$$X_d = \frac{24\mu_o(T_{ph}k_{w1})^2\omega RL}{\pi}\left(\frac{1}{g_2}+\left(\frac{1}{g_1}-\frac{1}{g_2}\right)\left(\beta+\frac{\sin\pi\beta}{\pi}\right)\right) \tag{32}$$

The synchronous reactance of the round rotor machine X_s can be easily deduced from (32) since $g_1 = g_2$ to yield

$$X_s = \frac{24\mu_o(T_{ph}k_{w1})^2\omega RL}{\pi g_o} \tag{33}$$

Equating (32) and (33) yields the expression for determining the aigrap g_o for the round rotor machine as

$$g_o = \frac{1}{(1/g_2)+\left((1/g_1)-(1/g_2)\right)\left(\beta+(\sin\pi\beta/\pi)\right)} \tag{34}$$

This gave an airgap value of $g_o = 0.34$ mm. The reactances of the salient pole machine were measured separately using slip test [17] as shown in Fig. 4*a*. The leakage reactance was estimated to be $X_{ls} = 3.1\ \Omega$ according to [15]. The two machines were then coupled together mechanically and then coupled to drive a dc generator feeding a variable resistive load through an RWT321 digital torque sensor. In the measurements carried out, two wattmetres were used to measure the input power from which power factor was calculated using

$$\cos\varphi = \cos\left(\tan^{-1}\left(\sqrt{3}\frac{W_1-W_2}{W_1+W_2}\right)\right) \tag{35}$$

Fig. 6 shows the experimental set up and the picture as used for the measurements. To ensure that the results were obtained under synchronous speed, a digital tachometer was used to measure the speed after each variation of load.

Owing to the narrow range of capacitive reactance in which high saliency ratio is obtainable (see Fig. 4*b*), a capacitance value of 58.1 μF was used. This choice leads a saliency ratio of about 20 and is guided by the values of currents each of the windings can support (not more than 3.7 A). A choice around the resonant peaks will ultimately lead to higher saliency ratio and improved performance but cannot be realised in practice because the windings cannot support the current that will flow in them and besides that will ultimately drive the machine into deep saturation. Prior to commencement of tests, the terminals X'–Y'–Z', *a*–*b*–*c* and *x*–*y*–*z* of Fig. 6 should be permanently short-circuited as applied to the rotor windings of an induction motor. In effect, three measurement sets based on the modification of the auxiliary winding circuit were made viz: open circuit, short circuit and connection of 58.1 μF capacitors. An open circuit is realised when the capacitors are removed and their

connection terminals left open. Only the main winding is in operation here. The short-circuit case is accomplished by shorting out the capacitors. A benchmark for these results is the torque and power factor characteristics of the salient pole half of the machine calculated when two of such machines are conventionally wound and coupled together. The results obtained from measurements are shown alongside the relevant calculated results in the following sections.

5.1 Power factor

The power factor of the hybrid machine is easily obtained from ac circuit theory as

$$\cos\varphi = \frac{\mathrm{Re}}{\sqrt{\mathrm{Re}^2 + Xe^2}} \tag{36}$$

For the same set of values of X_C as used before, a plot of power factor for a range of δ ranging from 0° to 45° is as shown in Fig. 7*a*. Here it is evident that the power factor appreciates for the hybrid machine as a capacitor is introduced. The power factor enhancement is higher at lower load angles.

5.2 Torque

The torque expression of this hybrid machine can be derived in several ways. We adapt the known results of conventional synchronous reluctance machine analysis and obtain the torque expression as

$$\begin{aligned} T_e &= \frac{3}{2}\frac{p_r}{2}\left(\left(\lambda_D I_Q - \lambda_Q I_D\right) + \left(\lambda_d I_q - \lambda_q I_d\right)\right) \\ &= \frac{V^2\left(2X_{md} - X_C\right)\left(X_{md} - X_{mq}\right)\sin 2\delta}{4X_{md}\left(X_c\left(X_{md} + X_{mq}\right) - 4X_{md}X_{mq}\right)} \end{aligned} \tag{37}$$

Two extreme cases can be considered viz: in the limit that $X_c \to 0$ (this implies short-circuiting the auxiliary winding), the torque expression resolves to

$$T_e\big|_{X_C \to 0} = \frac{3}{2}\frac{p_r}{2}\frac{V^2\left(X_{md} - X_{mq}\right)\sin 2\delta}{8X_{md}X_{mq}} \tag{38}$$

In the limit that $X_c \to \infty$ (implying the auxiliary winding is now open-circuited), the torque expression resolves to

$$T_e\big|_{X_C \to \infty} = \frac{3}{2}\frac{p_r}{2}\frac{V^2\left(X_{md} - X_{mq}\right)\sin 2\delta}{4X_{md}\left(X_{md} + X_{mq}\right)} \tag{39}$$

Both (38) and (39) give torque equations that show a relationship that is clearly similar to torque expressions of conventional synchronous reluctance machine as it is directly proportional to the reactance difference, $\sin 2\delta$ and square of the input voltage. Evidently, the torque equation of (38) is greater than that of (39) and provides the insight that the auxiliary winding contributes to the torque of the hybrid machine. Fig. 7*b* shows both the calculated and measured torque-angle plots. There is a marked simultaneous boost of power factor and torque by capacitance injection into the auxiliary winding of the hybrid machine as shown in Figs. 7*a* and *b* compared to the conventional machine.

5.3 Main and auxiliary winding currents

The currents flowing in both main and auxiliary windings under loading conditions are shown in Fig. 7*c* and *d*, respectively. While the main winding current gives a high full-load to no-load ratio as expected, the auxiliary winding current is nearly zero at no load under three conditions of measurements conducted ($X_c = \infty$, $X_c = 0$ and $C = 58.1$ μF). Expectedly, open-circuit conditions ($X_c = \infty$) displayed a zero auxiliary winding current throughout the entire loading. The sharp rise in the auxiliary winding current with load in under capacitive operation clearly displays that the machine operation (and by default, the value of capacitance that can be used in the auxiliary winding) will be conservatively be limited to current that the auxiliary winding can support. The capacitor voltage will be linearly related to the auxiliary winding current, ($V_c = I_a X_c$). A quick check can reveal that so long as the current rating of the auxiliary winding is not exceeded, the capacitor voltage will also remain within limits.

5.4 Output power and efficiency

The output power of the hybrid and the conventional benchmark machine can be readily construed to follow the trend of the calculated and measured torque profiles shown in Fig. 7*c* where it is evident that the hybrid machine renders an improved performance over the conventional machine. The machine efficiency for the entire range of measured and calculated operational variables shown in Fig. 7 can be computed if it is assumed that the iron loss P_i is constant at the calculated open-circuit no-load value of 106.81 W for the conventional machine and 131.95 W for the hybrid machine. Ignoring friction and stray load losses in both cases, the efficiency, η is given by

$$\eta = \frac{T_m \times \omega_r}{T_m \times \omega_r + P_i + P_{cu}} \tag{40}$$

In (40), T_m is the torque (in N m), ω_r is the synchronous speed (in rads/s) while P_{cu} is the sum of all the copper losses. For the conventional machine, the copper loss is calculated from the measured current in the stator winding while for the hybrid machine, it is calculated from the measured main and auxiliary winding currents. Since both windings are identical, P_{cu} (for the hybrid machine) can be found using

$$P_{cu} = 2 \times 3 \times \left(I_A^2 + I_a^2\right) r_s \tag{41}$$

Plots of measured and calculated efficiencies of the conventional and the hybrid machines are shown in Fig. 7*e*. Very close values of efficiency were recorded along the entire operating range. The efficiency of the hybrid machine is superior at lower load angles while at load angles beyond 17°, the efficiency of the conventional machine is better. These minor differences occurring in Fig. 7*e* can be clearly attributed to higher auxiliary winding currents of the hybrid machine at higher load angles. Specifically at a load angle of 22.5°, the efficiency of the conventional machine is 90.1% while that of the conventional machine is 91.21%. This difference is not considered significant in the presence of marginally higher power factors and torques rendered by

doi: 10.1049/iet-epa.2014.0149

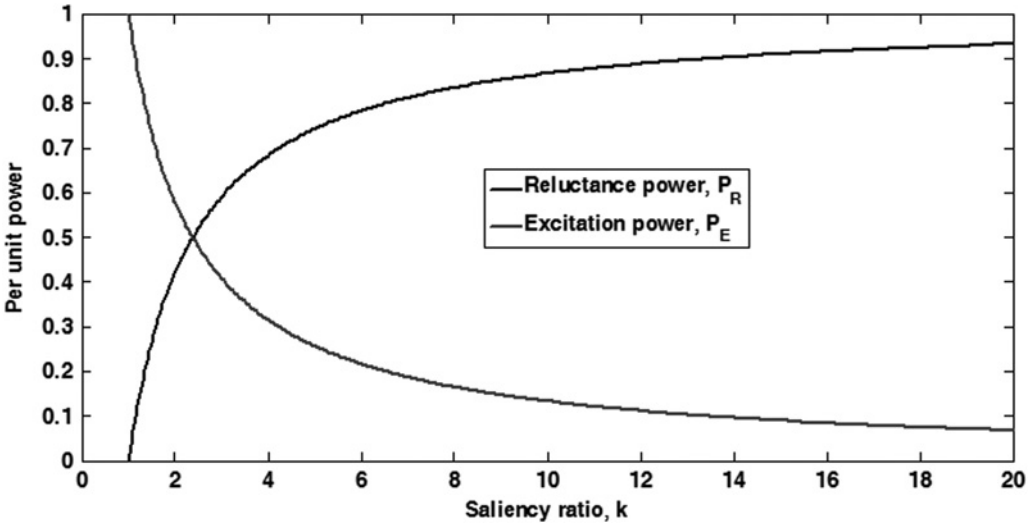

Fig. 8 *Percentage contribution of P_R and PE to PT for $1.0 \leq k \leq 10.0$*

the hybrid machine as seen in Figs. 7*a* and *b* and its ability to operate at lagging and leading power factors as earlier discussed.

6 Possible application of the hybrid machine for generation

In turbine generators say, there is always some inherent saliency although its contribution to the overall power output P_T is usually very small because of the low effective X_d/X_q ratio. Consider the output power of a turbine generator given as

$$P_T = P_E + P_R = \frac{3EV \sin\delta}{X_d} + \frac{3V^2}{2X_d}(k-1)\sin 2\delta \qquad (42)$$

where $k = X_d/X_q$ ratio.

The ratio of the reluctance power component, P_R to the overall power P_T for $E = 1.2$ pu and a conservative value of $\delta = 30°$ is

$$\frac{P_R}{P_T} = \frac{(\sqrt{3}/4)(k-1)}{0.6 + (\sqrt{3}/4)(k-1)} \qquad (43)$$

The percentage contributions of the reluctance power P_R and the excitation power, P_E to the overall output power P_T is as shown in Fig. 8 for various values of k.

It can be seen from Fig. 8 that for $k = 4$, say, the power contributed by reluctance is roughly twice the contribution because of the dc excitation. For very large value of k, the power component because of the dc excitation becomes negligible in comparison to that because of the reluctance. Dc excitation would nevertheless be required in order than the machine could operate as a stand-alone generator.

Suppose the rotor of the conventional turbine generator is modified by making the rotor partly salient and partly round, it should be possible to enhance the X_d/X_q ratio of the machine to any desired factor through capacitance loading of the auxiliary set of windings. The combined output because of the normal excitation and that because of the reluctance will produce more power, limited only by the conductor ratings and obviously a more stable and stiffer machine.

7 Conclusions

A hybrid synchronous reluctance machine with an ultra-high X_D/X_Q ratio at good power factors has been presented. The new machine is expected to have a relatively better asynchronous characteristic than a conventional synchronous reluctance machine because the difference between the rotor *d*-axis and *q*-axis reactances is not so pronounced as in a conventional synchronous reluctance machine. The pull-in torque, as a ratio of the pull-torque will therefore be greater. The stability of the machine on load can be raised by capacitance tuning after the machine has been brought to synchronism. It has been shown that the hybrid machine exhibits better performance than the conventional machine yielding better power factors at lower load angles and higher torque enhancement at higher load angles. These are only limited by the amount of current that the auxiliary windings can sustain. An optimality design therefore may require that auxiliary winding conductors be made slightly larger than the main windings conductors so that a higher capacitor value may be chosen for better performance.

The hybrid machine operating from a common busbar and not requiring dc excitation is expected to be a more robust and cheaper machine than the conventional synchronous generator as slip rings and excitation devices and their accessories will be completely eliminated. Absence of rotating windings will permit larger rotor diameter D which boosts the output power of the machine by a factor of D^2. Furthermore, it will permit the use of higher rotor speeds since centrifugal forces on the windings will be completely absent. If the number of poles of a given machine is halved from 4-pole to 2-pole, say, rotor speed as well as the output power will double for a given size of the rotor, resulting in a higher power density. Consequently, for a given mass of the rotor, the axial length of the machine could be shortened and this will eliminate some mechanical problems associated with long axial lengths like sagging and whirling. In addition, the inertia of the machine will increase and thus improve stability. The added effects of larger rotor diameter and increased speed can quadruple the

output power for a given machine size. The hybrid machine has power factor control, which could be made leading or lagging depending on the tuning of the capacitance loading of the auxiliary winding, a feature that cannot be accomplished in conventional synchronous reluctance machines. The machine line-start and stand-alone performances are being closely examined for motoring, generating and as synchronous condenser with a rotor possessing damper bars and field windings.

8 Acknowledgment

The authors are grateful to the management of Scientific Equipment Development Institute (SEDI), Akwuke-Enugu, Nigeria for machining the rotors used for this study to their designed shapes and sizes, and to the Alexander von Humboldt Foundation of Bonn, Germany for donating most of the measuring instruments used in the experiments.

9 References

1 Staton, D., Miller, T.J.E., Wood, S.E.: 'Maximizing the saliency ratio of the synchronous reluctance motor', *IEE Proc., B, Electr. Power Appl.*, 1993, **140**, (4), pp. 249–259
2 Wanlass, C.L.: 'US Patent 41887457', 5 February 1980
3 Umans, S.D., Hess, H.L.: 'Modeling and analysis of the Wanlass three-phase induction motor configuration', *IEEE Trans. Power Appl. Syst.*, 1983, **102**, (9), pp. 2912–26
4 Roberts, G.D.: 'US Patent 4808868', 28 February 1989
5 Medarametla, J.B., Cos, M.D., Baghzouz, Y.: 'Calculations and measurement of unity plus three-phase induction motor', *IEEE Trans. Energy Convers.*, 1992, **7**, (4), pp. 732–738
6 Obe, E.S., Senjyu, T.: 'Analysis of a polyphase synchronous reluctance motor with two identical stator windings', *Electr. Power Syst. Res. (EPSR)*, 2006, **76**, (6–7), pp. 515–524
7 Ogunjuyigbe, A.S.O., Jimoh, A.A., Nicolae, D.V., Obe, E.S.: 'Analysis of synchronous reluctance machine with magnetically-coupled three-phase windings and reactive power compensation', *IET Proc., Electr. Power Appl.*, 2010, **4**, (4), pp. 291–303
8 Obe, E.S.: 'Steady-state performance of a synchronous reluctance motor with capacitive assistance', *Electr. Power Syst. Res.*, 2010, **80**, pp. 1240–1246
9 Anih, L.U., Agu, L.A.: 'A novel strategy for raising the unit output of large synchronous machines', *Nigerian J. Technol.*, 2003, **22**, (1), pp. 24–28
10 Agu, L.A., Anih, L.U., Ojo, O., Jimoh, A.A.: 'Novel synchronous reluctance machines with capacitance injection'. LH Marthinusen Rotating Machine Conf., Pilansberg Conf. Centre, South Africa, 2005, pp. 1–8
11 Krause, P.C., Wasynczuk, O., Sudhoff, S.D.: 'Analysis of electric machinery' (IEEE Press, Piscataway, 2002)
12 Fuchs, E.F., Rosenberg, L.T.: 'Analysis of an alternator with two displaced stator windings', *IEEE Trans. Power Appar. Syst.*, 1974, **93**, (6), pp. 1776–1786
13 Schiferl, R.F., Ong, C.M.: 'Six phase synchronous machine with AC and DC stator connections, part I: equivalent circuit representation and steady-state analysis', *IEEE Trans. Power Appar. Syst.*, 1983, **PAS–102**, (8), pp. 2685–2693
14 Touma-Holmberg, M., Srivatava, K.: 'Double winding, high-voltage cable wound generator: steady-state and fault analysis', *IEEE Trans. Energy Convers.*, 2000, **19**, (12), pp. 245–250
15 Lloyd, T.C., Conrad, A.G., Puchstein, A.F.: 'Alternating-current machines' (Wiley, New York, 1958)
16 Lendenmann, H., Moghadam, R.R., Ari, T., Thand, L.-E.: 'Motoring ahead'. ABB Review, January 2011, pp. 56–61
17 Lawrenson, P.J., Agu, L.A.: 'Theory and performance of polyphase reluctance Machines'. Proc. IEE, 1964, vol. 111, no. 8, pp. 1435–45
18 Obe, E.S.: 'Measurement of Transient and Steady-State Load Angle in Synchronous Machines', Unpublished Masters of Engineering thesis, University of Nigeria, Nsukka, March 1999
19 Honsinger, V.B.: 'Steady-state performance of reluctance machines', *IEEE Trans. Power Appar. Syst.*, 1971, **PAS 90**, (1), pp. 305–317
20 Obe, E.S.: 'Small signal analysis of load angle governing and excitation control of ac generators', *Nigerian J. Technol.*, 2005, **24**, (2), pp. 1–15

doi: 10.1049/iet-epa.2014.0149